Intersubband Transitions in Nonpolar m-Plane AlGaN/GaN Heterostructures

Trang Nguyen, MohammadAli Shirazi-Hosseini-Dokht, Yang Cao, Rosa E. Diaz, Geoffrey C. Gardner, Michael J. Manfra, and Oana Malis*

Nonpolar AlGaN/GaN heterostructures have the potential to supplant polar heterostructures in infrared optoelectronic devices due to their theoretical advantages stemming from the absence of built-in polarization fields along nonpolar directions of the nitride wurtzite lattice. However, development of nonpolar m-plane infrared devices in a broad spectral range has been hampered, so far, by challenges to grow homogeneous high Al-composition AlGaN on m-plane GaN. $Al_xGa_{1-x}N$ layers with $0.6 < x < 0.8$ are found to be kinetically unstable under metal-rich growth conditions by plasma-assisted molecular-beam epitaxy. After reviewing recent progress in the field, this paper focuses on the effect of the structure of m-plane $Al_xGa_{1-x}N/GaN$ ($x < 0.6$) superlattices on near-infrared intersubband absorption. Even at these intermediate Al-compositions, the effective growth rate of AlGaN is drastically reduced, and the AlGaN-GaN interface roughness is unexpectedly high. Consequently, accurate determination of layer thicknesses and alloy composition necessitates structural characterization by a combination of scanning transmission electron microscopy and high-resolution X-ray diffraction. The energy and linewidth of near-infrared intersubband transitions are also significantly affected by this unusual growth behavior. The experimental results for intersubband absorption of m- and c-plane superlattices are compared to each other and with numerical calculations, and the main reasons for discrepancies are discussed.

1. Introduction

Nonpolar nitride heterostructures have been proposed as alternative materials to polar heterostructures for infrared intersubband (ISB) devices.[1–11] Due to large conduction band offsets between GaN and AlGaN, and large longitudinal-optical phonon energy, the nitrides are potential candidates for near- to far-infrared lasers and photodetectors. The advantages of nonpolar nitrides originate from the absence of built-in polarization fields that simplifies band structure engineering and maximizes wave-function overlap. For example, Feezell et al. compared the theoretical performance parameters of infrared photodetectors based on nonpolar and polar nitrides and found the nonpolar devices to have significantly higher absorption probability at low wavelengths.[12] This paper reviews recent progress in experimentally probing infrared intersubband transitions in m-plane AlGaN/GaN superlattices and efforts to theoretically model them. Special attention is given to the impact of the structure of high Al-composition AlGaN/GaN superlattices on near-infrared intersubband absorption.

Nonpolar nitride heterostructures have first attracted attention for applications in visible and ultra-violet light-emitting diodes. However, unavailability of high quality m-plane nitride substrates has delayed their use in other applications, such as infrared devices. Only recently, free-standing m-plane GaN substrates grown by hydride-vapor phase epitaxy have become commercially available and affordable enough for arduous growth studies. This is important because the growth on m-plane nitride heterostructures is markedly different from that of c-plane heterostructures. The differences are due to the anisotropy of adatom mobilities along the c- and a-direction on the m-plane surface during growth, to dangling bond geometries at step-edges, and to the anisotropic lattice mismatch between GaN and AlN along the c-direction (4%) and the a-direction (2.5%). Other factors specific to the crystal orientation may also affect the processes occurring on the surface during growth. Therefore, unlike the growth of c-plane AlGaN/GaN heterostructures that has been investigated extensively and is fairly well understood at this point, the growth of nonpolar m-

T. Nguyen, Y. Cao, Prof. O. Malis
Department of Physics and Astronomy
Purdue University
West Lafayette, Indiana 47907, USA
E-mail: omalis@purdue.edu

M. Shirazi-HD
School of Electrical and Computer Engineering
Purdue University
West Lafayette, Indiana 47907, USA

Dr. R. E. Diaz, Dr. G. C. Gardner
Birck Nanotechnology Center
West Lafayette, Indiana 47907, USA

Prof. M. J. Manfra
Department of Physics and Astronomy
School of Electrical and Computer Engineering
School of Materials Engineering
Birck Nanotechnology Center
West Lafayette, Indiana 47907, USA

plane heterostructures is still an active topic of research.[13–18] We have made significant progress in growing m-plane GaN and m-plane AlGaN/GaN superlattices with Al-composition below 20% that enabled us to observe THz intersubband absorption.[5] Others have also had success growing m-plane Al(Ga)N/GaN superlattices by different techniques in certain composition ranges.[2–10] However, it remains challenging to control the Al content of m-plane AlGaN over the full compositional range.

Mid-infrared intersubban absorption in m-plane AlGaN/GaN heterostructures grown by metal-organic chemical vapor deposition (MOCVD) was first reported by Kotani et al.[2–4] They examined the doping[3] and temperature[4] dependence of the intersubband transition energies. Lim et al. also demonstrated short- to long-wavelength infrared intersubband transitions in AlGaN/GaN heterostructures grown by molecular beam epitaxy (MBE).[6–9] Pesach et al. reported fabrication and performance of an m-plane InGaN/(Al)GaN quantum well infrared photodetector.[10] We first reported far-infrared (THz) intersubband absorption,[5] and then near-infrared absorption and photocurrent[11] in MBE-grown m-plane AlGaN/GaN superlattices. This paper focuses on our recent progress towards improving near-infrared intersubband absorption and understanding experimental observations.

2. Experimental Section

Our m-plane AlGaN/GaN superlattices were grown by plasma-assisted MBE on commercially available free-standing m-plane substrates from Nanowin, Inc. The substrates are either semi-insulating or n-type, have a typical root-mean-square (rms) roughness of 0.2–0.3 nm over $16\,\mu m^2$ and a nominal threading dislocation density of $< 2 \times 10^6 cm^{-2}$. The nominal miscut of the substrates is approximately 0.5° towards the $-c$ axis. This miscut was chosen based on previous work that showed it to be optimal for the surface morphology of MBE-grown m-plane GaN.[18] The rectangular substrates ($5 \times 10\,mm^2$) were mounted with liquid Ga on larger c-plane GaN-on-sapphire wafers. In some cases, a c-plane GaN template was co-loaded with the m-plane substrate to directly compare the structural parameters of the m- and c-plane superlattices grown simultaneously. All samples consist of 15-period AlGaN/GaN superlattices grown under metal-rich conditions with Ga/N ≈ 1.55. Gallium and aluminum fluxes were supplied by conventional effusion cells while nitrogen flux was provided by a Veeco Unibulb radio-frequency plasma source operating at 300W forward power with 0.5 sccm of nitrogen (N_2) flow. The structures were delta-doped in the barriers with silicon provided by an effusion cell. The substrate temperature is monitored with a pyrometer to be 720 °C. The growth rate of m-plane GaN is $8.8\,nm\,min^{-1}$ under these conditions and is equal, within measurement error, to that of c-plane GaN. **Table 1** summarizes the structural parameters and the results of optical measurements for a set of representative samples discussed below.

After growth, the samples were characterized by atomic force microscopy (AFM) and high-resolution x-ray diffraction (HRXRD). The HRXRD data was collected using a PANalytical X'Pert-MRD high-resolution x-ray diffractometer equipped with a four-bounce Ge monochromator. The HRXRD peak fits were performed assuming the growth rate of m-plane GaN layers to be
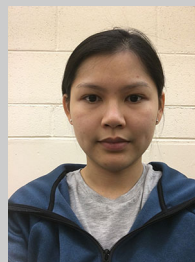
Trang Nguyen is pursuing a Ph.D. in Physics in the Dept. of Physics and Astronomy at Purdue University, currently focusing on the correlations between optical, electrical, and structural properties of different III-Nitride semiconductors. She is interested in studying various applications of nano-scale materials to help enhance the performance of existing instruments and designing new devices that work in the infrared (IR) and terahertz (THz) regimes. Trang Nguyen holds a B.S. in physics and math from the University of Michigan-Flint.

Michael J. Manfra is the Bill and Dee O'Brien Chair Professor of Physics and Astronomy, professor of electrical and computer engineering, and professor of materials engineering at Purdue University. His current research interests include: molecular beam epitaxy of ultra-high purity semiconductors, topological phases of matter, electronic transport at low temperatures and high magnetic fields in mesoscopic structures, and quantum computing. He joined the faculty of Purdue in 2009 after working for 10 years in the Semiconductor Physics Department of Bell Laboratories. He holds an A.B. in physics from Harvard University and a Ph.D. in physics from Boston University.

Oana Malis holds a M.S. Degree in physics from the University of Bucharest, Romania, and a Ph.D. in physics from Boston University. She started research on infrared materials and devices in 2003 at Bell Labs, Lucent Technologies. She continued her research on novel infrared materials first as an Assistant Professor in the Physics Dept. at SUNY Binghamton, and currently as an Associate Professor in the Dept. of Physics and Astronomy at Purdue University.

the same as for c-plane GaN. This assumption is supported by HRXRD and electron microscopy measurements of very low Al-composition AlGaN/GaN superlattices.[5,17] **Figure 1** shows the AFM surface scans, and the HRXRD $\omega/2\theta$ scans of the $(1\bar{1}00)$ and (0002) axis reflections of co-loaded m-plane and c-plane samples B and C, respectively. Narrow satellite peaks were observed confirming the existence of the superlattice structure. The presence and extent of pendellösung fringes are indicative of the superlattice thickness uniformity. These features are well

Table 1. Summary of structural parameters, and comparison of the experimental and theoretical values of the ISB transition energies, and integrated absorption for a set of representative m-plane and c-plane AlGaN/GaN superlattices whose ISB spectra are shown in **Figure 3**. The full-width-at-half-maximum (FWHM) of the experimental absorption curves is also listed.

Sample	Superlattice parameters (well/barrier nm)	Barrier material	Si delta Doping [cm^{-2}]	Calculated charge density [cm^{-2}]	ISB transition energy [meV]		Integrated absorption [meV]		FWHM [meV]
					Exp	Calc	Exp	Calc	Exp
A	m-plane 15 × 3.4/2.7	Al$_{0.45}$Ga$_{0.55}$N	2 × 1.04 · 10^{14}	2 · 10^{13}	388	399	88	161	124
B	m-plane 15 × 3.2/2.1	Al$_{0.56}$Ga$_{0.44}$N	2 × 2.3 · 10^{13}	2.4 · 10^{13}	340	462	89	154	159
C	c-plane 15 × 3.2/3.75	Al$_{0.23}$Ga$_{0.77}$N	2 × 2.3 · 10^{13}	8.4 · 10^{12}	272	301	70	52	109
D	m-plane 15 × 3.2/2.1	Al$_{0.54}$Ga$_{0.46}$N	2 × 1.15 · 10^{13}	2 · 10^{13}	429	474	69	151	177

reproduced by the dynamical theory of X-ray diffraction simulation performed with the commercial package PANalytical X'PERT EPITAXY (not shown in the figure).

Samples for scanning transmission electron microscopy (STEM) imaging and analysis were prepared using the focused ion beam (FIB) lift-out technique with a FEI Nova 200 DualBeam, and later thinned to transparency in a Nanomill at 900 eV. The STEM images were taken on a FEI Talos 200 kV with a Super X-EDS detector. **Figure 2** shows the STEM and EDX elemental maps for Ga and Al for sample A.

Near-infrared intersubband absorption measurements were performed using a Thermo Nicolet 8700 Fourier-transform infrared (FT-IR) spectrometer on samples polished into 45° multipass waveguides. All spectra display the normalized absorbance calculated following the procedure detailed in Refs. [19,20]. The electric-field overlap with the quantum wells (QWs) was estimated at the peak absorption wavelength, assuming a node at the air-semiconductor interface. Figure 3

shows a summary of the near-infrared ISB absorption of the representative samples listed in Table 1.

The band structures of the m-plane and c-plane AlGaN/GaN superlattices were calculated self-consistently using the eight-band k · p model, or a single band model for m-plane and c-plane structures, respectively, with the nextnano3 software.[21] **Figure 4** shows the calculated bare (i.e., uncorrected for many-body effects) conduction-band edge, ground, and first excited state probabilities calculated for samples B and C in Table 1. Many-body corrections were added to the transition energies according to the method presented in Ref. [22].

3. Results and Discussion

3.1. MBE Growth of m-Plane AlGaN/GaN Superlattices

Homogeneous m-plane Al$_x$Ga$_{1-x}$N with an Al composition between approximately 0.6–0.8 was found to be essentially unstable under Ga-rich growth conditions by plasma-enhanced MBE.[23] Specifically, we found that above a certain critical Al flux, growth of m-plane AlGaN under excess Ga leads to formation of inhomogeneous alloys with a unique nanostructure.[23] At high Al-fluxes, this nanostructure consists of continuous, nearly-pure AlN layers plus flat-top islands of lower Al-content bordered by m-plane nanofacets.[23] However, this nanostructure is undesirable for ISB devices and will not be discussed any further in this paper. Due to this growth instability, all infrared ISB measurements to date have been made using barriers with Al-composition either below 60%, or pure AlN barriers.[2–9] For the same reason, here we focus on examining the impact of the AlGaN structure on the near- to mid-infrared intersubband absorption of m-plane Al$_x$Ga$_{1-x}$N/GaN super-lattices with x < 0.6.

Even below 60% Al-composition, AlGaN growth on m-plane GaN differs substantially from c-plane growth. The average AlGaN growth rate drops rapidly with increasing Al beam flux under constant excess Ga flux. This behavior is
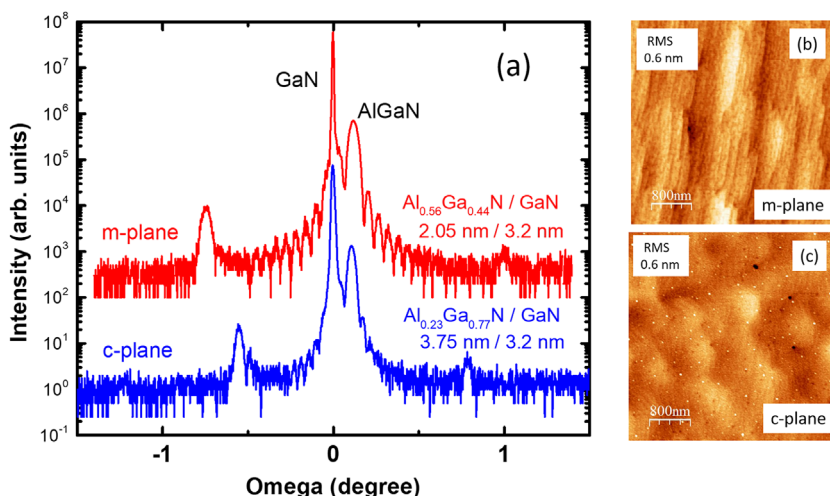

Figure 1. a) HRXRD in the vicinity of the (1100) and (0001) reflections for an m-plane (red curve) and c-plane (blue curve) AlGaN/GaN superlattices, respectively, grown simultaneously (samples B and C in Table 1). The angles are expressed relative to the corresponding GaN peaks. The two curves are shifted vertically for clarity. The text in (a) shows the results for the layer thicknesses and Al-composition from the fit of the HRXRD data (fit not shown). b) AFM of sample B. c) AFM of sample C.
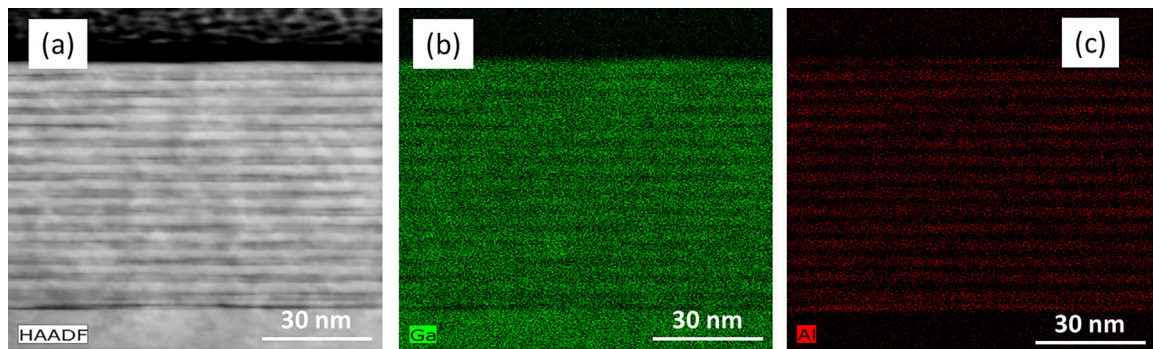
Figure 2. STEM (a) and EDX maps of Ga (green) (b) and Al (red) (c) for m-plane AlGaN/GaN superlattice sample A taken along the a-zone axis.

likely caused by the surface processes also responsible for the growth instability above 60% Al-composition. Its origin, though, is beyond the scope of this paper. Figure 1a shows a comparison of the HRXRD spectra of co-loaded m-plane sample B, and c-plane superlattice sample C. The QW and barrier widths listed on the plot were extracted from the fit of the HRXRD pattern (not shown in the figure) assuming the GaN growth rate is the same for both samples at $8.8 \, \text{nm} \, \text{min}^{-1}$. The drastic decrease of the m-plane AlGaN thickness (and associated growth rate) as compared to c-plane AlGaN thickness, is visible in the plot as an increase of the separation between superlattice satellite peaks (e.g., angular separation between AlGaN peak and superlattice peak on the left). The AlGaN m-plane barriers are significantly thinner than the c-plane counterparts (2 nm vs. 3.75 nm for m- and c-plane, respectively). This corresponds to an m-plane AlGaN growth rate of 4.4 nm min^{-1}, as opposed to the expected value of 8.8 nm min^{-1}. We note that the c-plane AlGaN growth rate was measured to be much closer to the GaN growth rate (8.1 nm min^{-1}). Simultaneously with the drop of growth rate, the average Al-composition (as established with HRXRD) increases super-linearly with Al beam flux.[23] The m-plane Al-composition is more than twice that of c-plane AlGaN (56% vs. 23% for m- and c-plane AlGaN, respectively). Therefore, accurate determination of the layer thicknesses and barrier composition requires a combination of STEM and HRXRD.

Figure 2 shows the STEM and EDX elemental maps for Ga and Al for sample A. It confirms that, under the growth conditions employed in this study, the GaN and AlGaN layers are fairly planar and do not exhibit the nanostructure of layer plus flat-top island that develops at higher Al-fluxes.[23] AFM scans shown in Figure 1b and c indicate that the top surfaces of both samples have similar roughness. However, the image in Figure 2a also reveals QW thickness variation and Al-composition fluctuations in the barriers that are more pronounced than in c-plane hetero-structures of similar composition.[19] For sample A, we could most accurately determine the average QW thickness (3.4 nm), and thickness distribution (standard deviation ≈ 0.5 nm). Note that for c-plane AlGaN/GaN superlattices, the QW width fluctuations are typically limited to less than two monolayers (standard deviation <0.25 nm).[1,19] Moreover, STEM line scans across the superlattice (not shown in Figure 2), and Ga, and Al EDX maps shown in Figure 2b and c, respectively, indicate Al-content variation of more than 10% in some barriers. However, the alloy composition variation occurs randomly, and therefore cannot be meaningfully quantified. The average QW thickness enabled the best agreement

between the measured near-infrared intersubband transition energy and calculated transition energy. STEM characterization, however, is technically challenging, and therefore, not feasible for each sample. Disagreement between optical transition measurement and calculations discussed below may, at least in part, be due to uncertainties of the structural parameters, when full STEM characterization is not available.

3.2. Comparison of Near-Infrared Optical Properties of m-Plane and c-Plane AlGaN/GaN Superlattices

Intersubband absorption in m-plane AlGaN/GaN has been reported in a wide spectral range from near-infrared to the terahertz range.[2–11] Due to the AlGaN growth instability at high Al-content, we focus our discussion here on superlattices containing less than 60%Al in the barriers. The MBE growth temperature that maximizes near-infrared ISB absorption of m-plane superlattices was determined to be 720 °C. We also found that modifying the doping profile by placing the Si-atoms into the barriers in 2 delta-doping sheets located at 1/3 and 2/3 of the
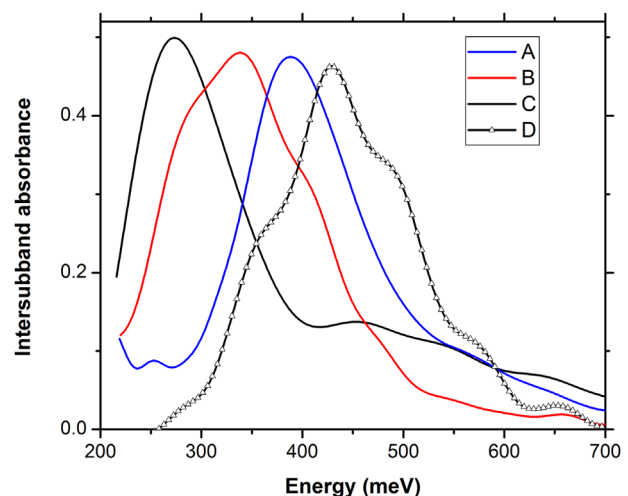

Figure 3. Near-infrared intersubband absorption spectra of a series of AlGaN/GaN superlattices. The red and black curves correspond to the co-loaded m-plane (B) and c-plane (C) samples, respectively, whose AFM and HRXRD are shown in **Figure 1**.
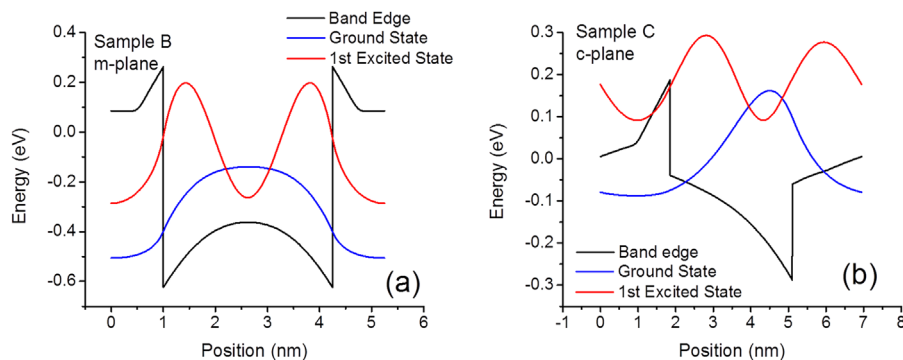
Figure 4. Conduction band edge and probability of the ground and first excited states for (a) m-plane sample B, and (b) c-plane sample C.

barrier thickness increases absorption amplitude and narrows linewidth as compared to the absorption of samples doped in the QWs. This effect can be explained by reduced impurity scattering in the case of barrier doping.

Near- to mid-infrared intersubband absorption was measured in m-plane AlGaN/GaN superlattices, and a brief comparison of the ISB absorbance of the representative structures listed in Table 1 is shown in Figure 3. The experimental results were compared with numerical calculations of the absorbance curves and with measurements of co-loaded c-plane samples. Figure 4 shows the calculated bare (i.e., uncorrected for many-body effects) conduction band edge, and wave-function probabilities for the ground and first excited states of co-loaded m-plane sample B and c-plane sample C. The wave-function probabilities are plotted in arbitrary units and offset on the vertical axis by the lowest energy of the respective subband. The main differences between the two types of samples stem from lower barrier height (consequence of lower Al-composition), and built-in polarization fields of sample C. Both effects result in lower bare transition energy for the c-plane structure. The calculated transition energies were then adjusted to include the effects of many-body corrections.[22]

For sample A, we obtained relatively good agreement between the measured transition energy and the energy calculated using the structural parameters established by a combination of STEM and HRXRD. Other authors also reported good agreement

between measurements and calculations.[2–4,6–9] However, this is not the case for all of our samples. For example, samples B and C were simultaneously grown on an m-plane and c-plane substrate, respectively, but good agreement with the calculated transition energy is only obtained for c-plane sample C. We note that good quantitative agreement has been found in the past for other c-plane AlGaN/GaN superlattices.[19] Furthermore, samples B and D have similar structural parameters, but significantly different transition energies that do not correlate well with calculated charge densities. Samples B and D were grown under different excess Ga conditions, though. We attribute the discrepancy between theoretical and measured ISB transition energies for some m-plane samples primarily to uncertainties in the knowledge concerning m-plane QW widths, and electron charge densities. The transition energy also depends indirectly on barrier height to the extent to which it affects barrier dopant activation.

The energy of ISB transitions in c-plane nitride superlattices was found to be extremely sensitive to QW thickness fluctuations.[1,19–20] This effect is accentuated in m-plane superlattices.[12] Single monolayer errors in the QW width could lead to ISB transition energy shifts of more than 20 meV. Due to $Al_xGa_{1-x}N$ surface roughness and alloy inhomogeneities even for $x < 0.6$, the uncertainty in the estimate of the QW width is larger for m-plane than for c-plane samples. Therefore, we believe this uncertainty to account at least in part for the
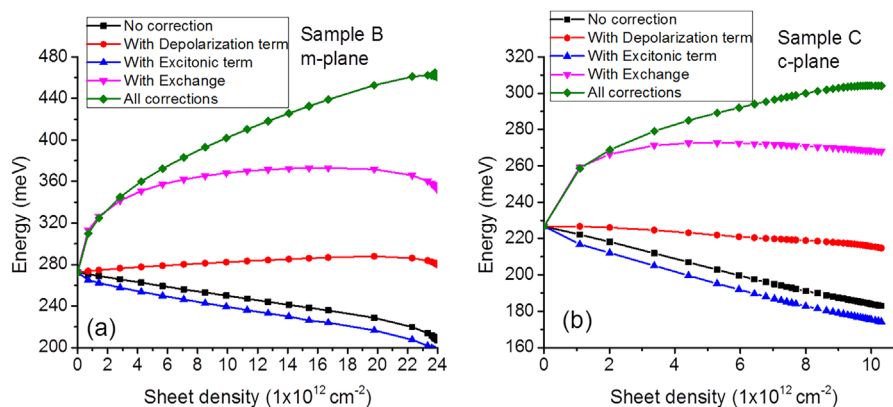

Figure 5. Comparison of many-body corrections as a function of sheet charge density for (a) the m-plane B, and (b) the c-plane C.

ADVANCED
SCIENCE NEWS

www.advancedsciencenews.com

physica
pss status solidi a

www.pss-a.com

differences between measured and predicted ISB transition energies. Moreover, QW width fluctuations are the main reason of inhomogeneous broadening of nitride ISB transitions. The full-width-at-half-maximum (FWHM) of ISB absorption curves for m-plane samples is larger than that of c-plane samples, for example, sample C, most likely due to the wider distribution of QW widths discussed in Section 3.1.

We also found that sheet charge density has a major effect on ISB transition energies in m-plane superlattices due to its effect on the many-body corrections. Therefore inaccuracies in sheet charge measurements and/or modeling can cause significant differences between experimental and calculated values of the transition energies. Kotani et al. were the first to discuss many-body corrections to the ISB absorption energies of m-plane AlGaN/GaN superlattices, but the many-body corrections to their transition energies were relatively small.[3] In contrast to their work that used an attenuated total reflectance technique, we found the need to significantly increase doping density in order to experimentally observe ISB absorption at higher energy in standard multipass waveguides.

Figure 5 shows the calculated dependence on sheet charge density of the different many-body corrections to the ISB transition energies in m-plane and c-plane AlGaN/GaN QWs with the structural parameters corresponding to samples B and C, respectively. The sheet density in the calculations was varied by changing the duration of the Si delta-doping. We found that the many-body corrections to the transition energies are substantially larger for m-plane samples than for c-plane samples even at the same charge density levels. For example, for a charge density of $1 \cdot 10^{13} \mathrm{cm}^{-2}$, the total correction to the transition energy of the m-plane sample B is 152 meV, while for sample C is 120 meV. The main difference between the two orientations at the same charge density is due to a larger exchange correction for the m-plane as compared to the c-plane structure. Furthermore, when the doping density is increased, the activated charge density in the c-plane QWs saturates to a lower value ($\approx 1 \cdot 10^{13} \mathrm{cm}^{-2}$) than for the m-plane QWs ($\approx 2.4 \cdot 10^{13} \mathrm{cm}^{-2}$). As a consequence, the model predicts a significantly larger active sheet charge for sample B than for sample C (see Table 1), even though they are both doped at the same level. Therefore, the predicted blue shift of the transition energy for the m-plane sample B (190 meV) is much larger than for the c-plane sample C (80 meV).

Experimentally, the ISB transition energy for sample B was found to be much lower than predicted, suggesting that the active charge density is much smaller than expected. The integrated intensities of the m-plane samples are also systematically lower than estimated theoretically, further supporting the assumption of reduced charge densities. In contrast, relatively good quantitative agreement was obtained for c-plane superlattices.[20] Smaller charge densities may be due to lower Si donor incorporation in m-plane AlGaN as compared to c-plane AlGaN, or to considerably higher activation energy due to increased Al-content in the alloy. The activation energy of Si in high-Al content c-plane AlGaN is still a matter of active investigation.[24] Fermi-level pinning on the surface can also lead to charge depletion from the superlattice.[18] Relatively little is known about activation energies and surface Fermi-level pinning of m-plane AlGaN. Moreover, charge trapping by point and extended defects could also play a role in reducing electron density. These processes are typically sensitive to growth conditions, such as excess Ga, and therefore may be the reason for differences between the absorption spectra of samples with nominally identical structural parameters, such as B and D. Considerably more experimental (charge density measurements, defect identification, etc.) and theoretical research (many body corrections beyond perturbative approach) needs to be done to clarify these issues.

4. Conclusions

Nonpolar m-plane AlGaN/GaN heterostructures have the potential to enable novel infrared optoelectronics devices. Significant progress has been made towards growing them and studying their optical properties in a broad spectral range covering the technologically important near- and far-infrared. This paper reviewed the results reported in the literature, and discussed in detail some of the challenges currently limiting our understanding of near-infrared intersubband absorption in m-plane AlGaN/GaN superlattices with Al-composition below 60% grown by MBE. Most importantly, the structure of m-plane AlGaN is significantly different from the structure of c-plane AlGaN when grown under identical Ga-rich conditions by MBE. Even at relatively low Al-fluxes that typically result in growth of low-Al containing c-plane $Al_xGa_{1-x}N$ ($x < 0.3$), the m-plane AlGaN exhibits a drastically reduced growth rate, considerably higher Al-content ($x > 0.5$), increased interface roughness, and pronounced alloy inhomogeneity. By comparing structural and optical properties of co-loaded m- and c-plane structures, we concluded that uncertainties in determining QW width and charge density explain most of the quantitative discrepancies between experimental and calculated ISB transition energies of m-plane samples. Moreover, quantum-well thickness fluctuations result in wider ISB absorption features of m-plane heterostructures. Future progress depends on our ability to further optimize heterostructure growth to alleviate current material issues by any available growth technique (MBE or MOCVD). In MBE, this may be achieved through careful control of growth conditions, and substrate miscut. MOCVD may allow access to a completely different set of growth conditions, but no exhaustive investigations of the growth of m-plane AlGaN/GaN superlattices by this technique have been reported to date. Better understanding of impurity incorporation, and improved modeling of many-body corrections to ISB transition energies are also essential to accurately predicting and explaining the performance of nonpolar nitrides in infrared optoelectronics.

Conflict of Interest

The authors declare no conflict of interest.

[1] M. Beeler, E. Trichas, E. Monroy, *Semicond. Sci. Technol.* **2013**, *28*, 074022.

[2] T. Kotani, M. Arita, Y. Arakawa, *Appl. Phys. Lett.* **2014**, *105*, 261108.

[3] T. Kotani, M. Arita, Y. Arakawa, *Appl. Phys. Lett.* **2015**, *107*, 112107.

[4] T. Kotani, M. Arita, K. Hoshino, Y. Arakawa, *Appl. Phys. Lett.* **2016**, *108*, 052102.

[5] C. Edmunds, J. Shao, M. Shirazi-HD, M. J. Manfra, O. Malis, *Appl. Phys. Lett.* **2014**, *105*, 021108.

[6] C. B. Lim, M. Beeler, A. Ajay, J. Lahnemann, E. Bellet-Amalric, C. Bougerol, E. Monroy, *J. Appl. Phys.* **2015**, *118*, 014309.

[7] C. B. Lim, A. Ajay, C. Bougerol, B. Hass, J. Schormann, M. Beeler, J. Lahnemann, M. Eickhoff, E. Monroy, *Nanotechnology* **2015**, *26*, 435201.

[8] C. B. Lim, A. Ajay, C. Bougerol, J. Lahnemann, F. Donatini, J. Schormann, E. Bellet-Amalric, D. A. Browne, M. Jimenez-Rodriguez, E. Monroy, *Nanotechnology* **2016**, *27*, 145201.

[9] C. B. Lim, M. Beeler, A. Ajay, J. Lahnemann, E. Bellet-Amalric, C. Bougerol, J. Schormann, M. Eickhoff, E. Monroy, *Jap. J. Appl. Phys.* **2016**, *55*, 05FG05.

[10] A. Pesach, E. Gross, C.-Y. Huang, Y.-D. Lin, A. Vardi, S. E. Schacham, S. Nakamura, G. Bahir, *Appl. Phys. Lett.* **2013**, *103*, 022110.

[11] O. Malis, C. Edmunds, D. Li, J. Shao, G. Gardner, W. Li, P. Fay, M. J. Manfra, Novel In-Plane Semiconductor Lasers XIII, edit. by Alexey A. Belyanin, Peter M. Smowton, Proc. of the SPIE 2014 **2014**, *9002*, 90021D.

[12] D. Feezell, Y. Sharma, S. Krishna, *J. Appl. Phys.* **2013**, *113*, 1133103.

[13] M. Sawicka, H. Turski, M. Siekacz, J. Smalc-Koziorowska, M. Krysko, I. Dziecielewski, I. Grzegory, C. Skierbiszewski, *Phys. Rev. B* **2011**, *83*, 245434.

[14] M. Sawicka, C. Cheze, H. Turski, J. Smalc-Koziorowska, M. Krysko, S. Kret, T. Remmele, M. Albrecht, G. Cywinski, I. Grzegory, C. Skierbiszewski, *J. Cryst. Growth* **2013**, *377*, 184.

[15] J. Smalc-Koziorowska, M. Sawicka, T. Remmele, C. Skierbiszewski, I. Grzegory, M. Albrecht, *Appl. Phys. Lett.* **2011**, *99*, 061901.

[16] M. Sawicka, A. Feduniewicz-Żmuda, H. Turski, M. Siekacz, S. Grzanka, M. Kryśko, I. Dzięcielewski, I. Grzegory, C. Skierbiszewski, *J. Vac. Sci. Technol. B* **2011**, *29*, 03C135.

[17] J. Shao, L. Tang, C. Edmunds, D. Zakharov, O. Malis, M. J. Manfra, *Appl. Phys. Lett.* **2013**, *103*, 232103.

[18] J. Shao, L. Tang, C. Edmunds, G. Gardner, O. Malis, M. J. Manfra, *J. Appl. Phys.* **2013**, *114*, 023508.

[19] C. Edmunds, L. Tang, J. Shao, D. Li, M. Cervantes, G. Gardner, D. N. Zakharov, M. J. Manfra, O. Malis, *Appl. Phys. Lett.* **2012**, *101*, 102104.

[20] C. Edmunds, L. Tang, M. Cervantes, M. Shirazi-HD, J. Shao, A. Grier, A. Valavanis, J. D. Cooper, D. Li, G. Gardner, D. N. Zakharov, Z. Ikonic, D. Indjin, P. Harrison, M. J. Manfra, O. Malis, *Phys. Rev. B* **2013**, *88*, 235306.

[21] S. Birner, T. Zibold, T. Andlauer, T. Kubis, M. Sabathil, A. Trellakis, P. Vogl, *IEEE Trans. Electron Devices* **2007**, *54*, 2137.

[22] M. Tchernycheva, L. Nevou, L. Donyennette, F. H. Julien, E. Warde, F. Guilliot, E. Monroy, E. Bellet-Amalric, T. Remmele, M. Albrecht, *Phys. Rev. B* **2006**, *73*, 125347.

[23] M. Shirazi-HD, R. E. Diaz, T. Nguyen, J. Jian, G. C. Gardner, H. Wang, M. J. Manfra, O. Malis, *J. Appl. Phys.* **2018**, *123*, 161581.

[24] R. Collazo, S. Mita, J. Xie, A. Rice, J. Tweedie, R. Dalmau, Z. Sitar, *Phys. Status Solidi C* **2011**, *8*, 2031.